AIP Applied Physics Letters

Tunable Fano resonances based on two-beam interference in microring resonator

Ting Hu, Ping Yu, Chen Qiu, Huiye Qiu, Fan Wang et al.

Citation: Appl. Phys. Lett. **102**, 011112 (2013); doi: 10.1063/1.4773917
View online: http://dx.doi.org/10.1063/1.4773917
View Table of Contents: http://apl.aip.org/resource/1/APPLAB/v102/i1
Published by the American Institute of Physics.

Tunable Fano resonances based on two-beam interference in microring resonator

Ting Hu,[1,2] Ping Yu,[1] Chen Qiu,[1] Huiye Qiu,[1] Fan Wang,[3] Mei Yang,[1,4] Xiaoqing Jiang,[1] Hui Yu,[1,a)] and Jianyi Yang[1,2,b)]

[1]*Department of Information Science and Electronic Engineering, Zhejiang University, Hangzhou 310027, China*
[2]*Cyrus Tang Center for Sensor Materials and Applications, Zhejiang University, Hangzhou 310027, China*
[3]*Suzhou Institute of Biomedical Engineering and Technology, Chinese Academy of Sciences, Suzhou 215163, China*
[4]*Department of Electrical and Computer Engineering, University of Nevada, Las Vegas, Nevada 89154, USA*

(Received 9 November 2012; accepted 17 December 2012; published online 7 January 2013)

In this paper, a resonant system is demonstrated on silicon-on-insulator wafer to achieve tunable Fano resonances. In this system, the Fano resonance originates from the interference of two beams resonant in the microring resonator. The shapes of the Fano resonances are tunable through controlling the phase difference of the two beams. Both large slope and high extinction ratio (ER) are obtained when the phase difference is 0.5π or 1.5π. Experimental results show that Fano resonances with steep slope and ER over 20 dB are achieved in the whole free spectral range by controlling the microheaters to meet the phase condition. © *2013 American Institute of Physics*. [http://dx.doi.org/10.1063/1.4773917]

Fano resonance,[1] which results from interference between a resonance pathway and a coherent background pathway, has attracted broad research interests due to its potential application in high-sensitivity sensing and low power optical switching/modulating. A lot of theoretical and experimental works have been done to obtain the sharp asymmetric Fano resonances.[2–19] In Ref. 2, Fan proposed the side-coupled waveguide-cavity systems to generate sharp Fano resonance and proved that its performance is greatly improved compared to the counterpart with symmetric line shape. Based on this model, Chao and Guo experimentally demonstrated the sensitive biochemical sensors.[4] Mario *et al.* composed a two-ring resonator configuration to produce sharp Fano resonances to provide the optical switching with high extinction ratio (ER), large modulation depth (MD), and low switching threshold. The advantages compared with the conventional one-ring configuration were also considered in this work.[6] Recently, Li *et al.* showed the possibility to control the Fano resonance in indirectly coupled whispering-gallery micro-resonators.[13]

The transmission spectrum of a single microring resonator (MRR) typically exhibits symmetric Lorentz line shape. But if two coherent lights (phase difference is not equal to 0 or π) are sent into the MRR simultaneously, the interference of the two beams destroys the optical power's symmetric distribution on the two sides of the resonant wavelength, and subsequently leads the transmission spectrum to be an asymmetric Fano resonance. In this letter, we design and demonstrate a microring resonator-based two-beam interferometer (MRR-TBI) on silicon-on-insulator (SOI) to produce tunable Fano resonances. Two microheaters are addressed to tune the line shapes and resonant wavelengths, respectively, by utilizing the thermo-optic (TO) effect of silicon. The relationship between the spectral slope and phase difference of the two beams is theoretically analyzed. Based on the analysis results, by controlling the two heaters, we can obtain the Fano resonances with both steep slope and relative high ER over the whole free spectral range (FSR).

The schematic structure of the MRR-TBI, as shown in Fig. 1(a), consists of a 1×2 multi-mode interference (MMI) power splitter and a MRR. The two arms of the MMI splitter are also the bus waveguides of the MRR. The two coupling regions have the field coupling coefficient of k_1 and k_2. In the configuration, the input beam will be divided to two parts by the 1×2 MMI splitter and then partly coupled into the MRR through the two coupling zones. E_{i1} and E_{i2} are the electric fields of the input bus waveguides, while E_{o1} and E_{o2} represent that of the output bus waveguides. The optical transmission spectra of the output ports can be derived by the transfer matrix method[20,21] as

$$P_{o1}=|E_{o1}|^2=\left|\frac{t_1-t_2\,\alpha\exp(j\theta)}{1-\alpha\,t_1t_2\exp(j\theta)}\cdot\gamma^{\frac{1}{2}}+\alpha_c\cdot\frac{-\alpha^{\frac{1}{2}}k_1k_2\exp\left(\frac{j\theta}{2}\right)}{1-\alpha\,t_1t_2\exp(j\theta)}\cdot(1-\gamma)^{\frac{1}{2}}\cdot\exp(j\varphi)\right|^2,$$

$$P_{o2}=|E_{o2}|^2=\left|\alpha_c\cdot\left(\frac{-\alpha^{\frac{1}{2}}k_1k_2\exp\left(\frac{j\theta}{2}\right)}{1-\alpha\,t_1t_2\exp(j\theta)}\cdot\gamma^{\frac{1}{2}}+\alpha_c\cdot\frac{t_2-t_1\alpha\exp(j\theta)}{1-\alpha\,t_1t_2\exp(j\theta)}\cdot(1-\gamma)^{\frac{1}{2}}\cdot\exp(j\varphi)\right)\right|^2, \quad (1)$$

a)Electronic mail: afterglow.yuhui@gmail.com.
b)Electronic mail: yangjy@zju.edu.cn.

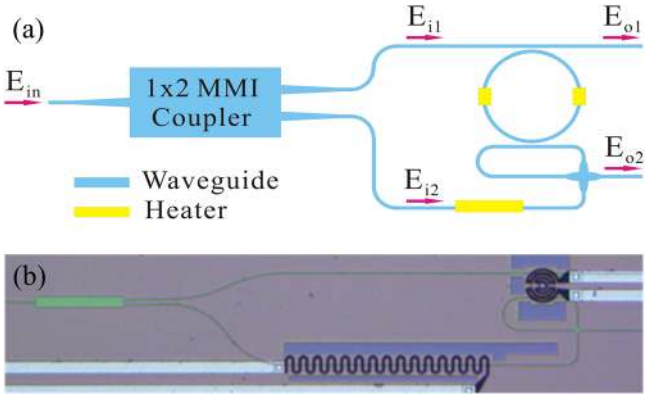

FIG. 1. (a) Schematic structure and (b) optical micrograph of the MRR-TBI.

where α and α_c are the single-pass amplitude attenuation factors of the ring and crossing waveguide, respectively. φ and γ are the phase difference and power ratio between E_{i1} and E_{i2}. The coupling between the bus and ring waveguides is assumed lossless so that the self and cross coupling coefficients k and t satisfy $k_i^2 + t_i^2 = 1$ ($i = 1, 2$). $\theta = 4\pi^2 n_{eff} R/\lambda$, is the single-pass phase shift of the ring, where R is the radius of the ring, λ is the optical wavelength, and n_{eff} is the effective refractive index of waveguides.

In the ideal condition, the input light will be divided to two beams with equal power, so γ is assumed to be 0.5. According to Eq. (1), the calculated transmission spectra of P_{o1} and P_{o2} at the resonance around 1544.4 nm are shown in Fig. 2. We can see from the figures that both the Fano-resonance line shapes of P_{o1} and P_{o2} vary with φ, except when $\varphi = 0$ or $\varphi = \pi$ the transmission line shapes exhibit symmetric profiles. Notice that the spectra for P_{o1} (P_{o2}) at $\varphi = \zeta$ (ζ is an arbitrary angle from 0 to 2π) and $\varphi = 2\pi - \zeta$ are horizontal mirror-symmetric. Obviously, the Fano-resonance line shapes can be controlled by tuning the value of φ. In the simulation, $k_1 = k_2 = 0.25$, $\alpha = 0.9928$, and $\alpha_c = 0.95$ are assumed, respectively.

The physical dimension of the MRR-TBI is determined by the numerical simulation. The structure optimizing the

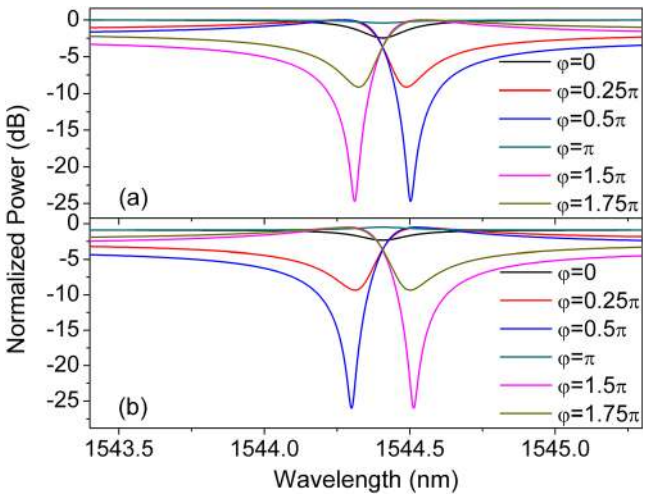

FIG. 2. Calculated transmission spectra of (a) P_{o1} and (b) P_{o2} of the MRR-TBI.

1×2 MMI splitter is simulated by employing the three-dimensional beam propagation method (BPM). The width and length of the MMI waveguide, in which the self-image effect happens, are 9 and 75.25 μm, respectively. The input port is located at the center of the left side, while the two output ports are set 2.25 μm away from the center at the right side. A 40-μm-long linear tapered waveguide provides an adiabatic transition between the interconnecting waveguides and the 1.2-μm-wide MMI access waveguides. The interconnecting and ring waveguides are designed with a cross section of 450×220 nm^2 and all waveguides are with a 60-nm-thick slab. The 10-μm-radius ring is chosen to obtain a FSR around 10 nm. The relationship of the coupling coefficient and the gap between bus and ring waveguides are calculated using three-dimensional finite-difference time-domain (FDTD) method. The gap of 300 nm is selected to obtain a trade-off among the ER, optical bandwidth, and drop insertion loss of the MRR. The FDTD method is also employed to optimize the ellipse-based crossing waveguide in the lower output arm of the MMI splitter. For realizing low transmission loss and lateral crosstalk, the long and short axes of that are chosen to be 8 and 2 μm, respectively. To control the Fano-resonance line shapes, one microheater (H_1) is placed over the lower arm of the MMI splitter to change φ through TO effect. Another microheater (H_2) over the ring is proposed to tune the resonant wavelength of the Fano resonance.

The device is fabricated on a SOI wafer with 220-nm-thick top silicon layer and 2-μm-thick buried dioxide layer. The 248-nm deep ultraviolet (UV) photolithography is used to define the device pattern. Inductively coupled plasma etching process is adopted to etch the top silicon layer. The grating couplers, covering layer, via, 120-nm-thick TiN microheaters, aluminum wires, and pads are fabricated with the same process in Refs. 22 and 23. The top-view optical micrograph of a typical fabricated device is shown in Fig. 1(b).

The fabricated device is characterized by using an amplified spontaneous emission (ASE) source, an optical spectrum analyzer (OSA), and two tunable voltage sources. The broadband light is coupled into the device through the grating coupler. The output light is collected by another grating coupler and fed into the OSA. The two voltage sources are used to drive the two TiN heaters. Fig. 3(a) shows the measured TE-polarized (electric field parallel to the chip) transmission spectra for the two output ports without biasing H_1 and H_2. Both P_{o1} and P_{o2} exhibit asymmetric resonant line shapes. Due to the transmission loss caused by the crossing waveguide, the insertion loss of the p_{o2} is larger than that of P_{o1}. The Fano resonance of P_{o1} reaches an ER $\sim$ 20 dB, which is slightly smaller than that of P_{o2}. The quality factor is observed to be around 1.08×10^4. To tune the line shapes, biases of 6 to 10 V with 1 V increment are applied to H_1. The measured transmission spectra are shown in Figs. 3(b)–3(f). At 9 V bias, near symmetric spectra are observed. As the voltage increases continuously, as shown in Fig. 3(f), the transmission spectra become Fano resonances again. But the line shapes trend to be swapped compared to those with bias under 9 V. In order to accurately control the Fano line shapes, we fit the measured transmission spectra by using Eq. (1), to analyze the value of φ. The corresponding

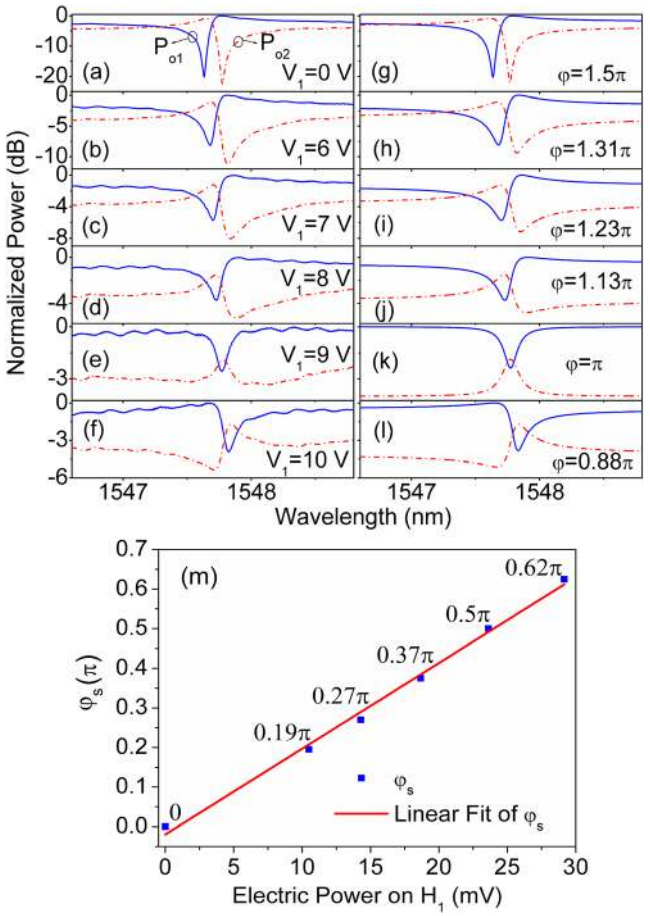

FIG. 3. (a)–(f) Measured output-port transmission spectra of the MRR-TBI with various bias voltages on H_1. (g)–(l) Modeled corresponding output-port transmission spectra. (m) Analyzed TO effect-induced phase shifts.

modeled spectra for Figs. 3(a)–3(f) are shown in Figs. 3(g)–3(l), with $\varphi = 1.5\pi$, 1.31π, 1.23π, 1.13π, π, and 0.88π, respectively. Here, we adopt $\alpha = 0.9924$, $\gamma = 0.5$, $\alpha_c = 0.922$, and $k_i = 0.2$ ($i = 1, 2$), and find good agreement between the measured and modeled spectra. The fit values of α_c and k_i decrease slightly when the applied voltage is large. This may attribute to the thermal crosstalk affecting the crossing waveguide's transmission loss and the MRR's coupling. The analyzed TO effect-induced phase shifts (φ_s) by heater H_1 (3.43 kΩ) are shown in Fig. 3(m). The linear fit line of φ_s illustrates that it approximately increases linearly with increasing the applied electric power on H_1, which makes the exact control of the Fano line shape feasible.

Since the sharp asymmetric line shape can greatly reduce the required phase change for high-sensitivity sensing or low power optical switching/modulating, it is important to control the Fano-resonance spectra achieving large slope, meanwhile, with a relative high ER. The slopes of P_{o1} and P_{o2} at the resonant wavelengths ($\theta = 2m\pi$, m is an integer) can be derived from Eq. (1) as

$$S_1 = \frac{\alpha_c[\alpha\gamma(1-\gamma)]^{\frac{1}{2}} k_1 k_2 (t_1 + \alpha t_2)\sin\varphi}{(1-\alpha t_1 t_2)^2},$$
$$S_2 = \frac{\alpha_c{}^3[\alpha\gamma(1-\gamma)]^{\frac{1}{2}} k_1 k_2 (\alpha t_1 + t_2)\sin\varphi}{(1-\alpha t_1 t_2)^2}. \quad (2)$$

It is clear, from Eq. (2), when φ is equal to $\pi/2$ or $3\pi/2$, slopes have the maximum value. According to previous theoretical analysis, the line shapes of P_{o1} (P_{o2}) at $\varphi = \pi/2$ and $\varphi = 3\pi/2$ are mirror-symmetric. Thus, tuning the transmission spectra to be the same or mirror-symmetric with that shown in Fig. 3(a) can obtain a sharp asymmetric line shape with an ER over 20 dB. Figs. 4(a) and 4(b) display the Fano resonant wavelengths of P_{o1} and P_{o2} tuned over the whole FSR by utilizing H_2 to heat the MRR. Because of the wavelength dispersion of n_{eff}, φ for each resonance is different, which leads those resonances to present various shapes. By controlling H_1 to compensate the phase shift caused by the wavelength dispersion, sharp Fano resonances with ER over 20 dB are obtained in the whole FSR (Figs. 4(c) and 4(d)). The applied voltages on H_2 for shifting the resonant wavelength and on H_1 for achieving the sharp line shape are listed in Table I.

In Figs. 4(a) and 4(b), resonances #3 and #5 have the similar gesture, but after tuned to sharp line shapes, they become mirror-symmetric gesture, as shown in Figs. 4(c) and 4(d). It is because that φ at #3 is close to but less than 2π, while φ at #5 is close to but larger than π. As voltage is applied to H_1, φ decreases. At #3, it decreases to $3\pi/2$ without pasting the gesture flip point ($\varphi = 0$ or π). Oppositely, φ at #5 decreases to $\pi/2$ and pasts the gesture flip point ($\varphi = \pi$), thus the gesture is changed. To resolve the problem, we can add one more heater over the other output arm of the MMI splitter so that it is flexible to increase or decrease φ rather than can only decrease it in our demonstrated device.

In summary, we experimentally demonstrate a MRR-TBI that can generate Fano resonances. The device is fabricated on SOI wafer by the complementary metal-oxide-semiconductor (CMOS) compatible process. The Fano-resonance line shapes are well controlled by tuning the phase difference between the two lights fed into the MRR through the TO effect of silicon. By utilizing the heaters H_1 and H_2 to satisfy the phase condition, Fano resonances are tuned to those with sharp slope and ER over 20 dB in the whole FSR, which leads the fabricated device potential to apply in high-sensitivity sensing and low power optical switching/modulating.

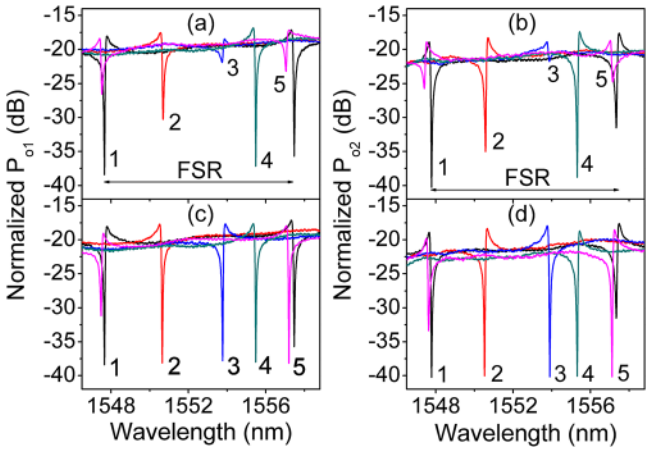

FIG. 4. Measured output-port transmission spectra of the MRR-TBI (a) and (b) before and (c) and (d) after tuned to be sharp line shapes with high ER over the whole FSR.

TABLE I. Voltages applied on H_1 and H_2.

Fano resonance	#1	#2	#3	#4	#5
V_{H_1} (V)	0	3.65	8.16	0	10.55
V_{H_2} (V)	0	5.5	8	9.02	10

This work was supported by the Natural Science Foundation of China under Grant Nos. 60977043, 61007063, and 61228501, the 863 project under Grant No. 2012AA012203, and Tang Zhongyin Fund.

[1]U. Fano, Phys. Rev. **124**, 1866 (1961).
[2]S. Fan, Appl. Phys. Lett. **80**, 908 (2002).
[3]S. Fan and W. Suh, J. Opt. Soc. Am. A **20**, 569 (2003).
[4]C.-Y. Chao and L. J. Guo, Appl. Phys. Lett. **83**, 1527 (2003).
[5]Y. Lu, J. Yao, X. Li, and P. Wang, Opt. Lett. **30**, 3069 (2005).
[6]L. Y. Mario, S. Darmawan, and M. K. Chin, Opt. Express **14**, 12770 (2006).
[7]L. Zhou and A. W. Poon, Opt. Lett. **32**, 781 (2007).
[8]F. Wang, X. Wang, H. Zhou, Q. Zhou, Y. Hao, and X. Jiang, Opt. Express **17**, 7708 (2009).
[9]A. E. Miroshnichenko and Y. S. Kivshar, Rev. Mod. Phys. **82**, 2257 (2010).
[10]A. C. Ruege, S. Member, R. M. Reano, and S. Member, J. Lightwave Technol. **28**, 2964 (2010).
[11]X. Xiao, J. Wu, F. Miyamaru, M. Zhang, and S. Li, Appl. Phys. Lett. **98**, 011911 (2011).
[12]R. Singh, I. A. I. Al-Naib, M. Koch, and W. Zhang, Opt. Express **19**, 6312 (2011).
[13]B.-B. Li, Y.-F. Xiao, C.-L. Zou, X.-F. Jiang, and Y.-C. Liu, Appl. Phys. Lett. **100**, 021108 (2012).
[14]C. Qiu, P. Yu, T. Hu, F. Wang, X. Jiang, and J. Yang, Appl. Phys. Lett. **101**, 021110 (2012).
[15]R. Singh, I. A. I. Al-Naib, M. Koch, and W. Zhang, Opt. Express **18**, 13044 (2010).
[16]R. Singh, X. Lu, J. Gu, Z. Tian, and W. Zhang, J. Opt. **12**, 015101 (2010).
[17]R. Singh, I. A. I. Al-Naib, Y. Yang, D. R. Chowdhury, W. Cao, C. Rockstuhl, T. Ozaki, R. Morandotti, and W. Zhang, Appl. Phys. Lett. **99**, 201107 (2011).
[18]W. Cao, R. Singh, I. A. I. Al-Naib, M. He, A. J. Taylor, and W. Zhang, Opt. Lett. **37**, 3366 (2012).
[19]J. Gu, R. Singh, X. Liu, X. Zhang, Y. Ma, S. Zhang, S. A. Maier, Z. Tian, A. K. Azad, H. Chen, A. J. Taylor, J. Han, and W. Zhang, Nature Commun. **3**, 1151 (2012).
[20]A. Yariv, Electron. Lett. **36**, 321 (2000).
[21]A. Yariv, IEEE Photon. Technol. Lett. **14**, 483 (2002).
[22]T. Hu, H. Qiu, P. Yu, C. Qiu, W. Wang, X. Jiang, M. Yang, and J. Yang, Opt. Lett. **36**, 4710 (2011).
[23]T. Hu, W. Wang, C. Qiu, P. Yu, H. Qiu, Y. Zhao, and X. Jiang, IEEE Photon. Technol. Lett. **24**, 524 (2012).